Mechanism for Si Poisoning of Al-Ti-B Grain Refiners in Al-Alloys

Yun Wang [a], Zhongping Que [a], Teruo Hashimoto [b], Xiaorong Zhou [b], Zhongyun Fan [a]*

a BCAST, Brunel University London, Uxbridge, Middlesex, UB8 3PH, UK

b School of Materials, University of Manchester, Manchester, M13 9PL, UK

* Corresponding author:

Professor Zhongyun Fan
BCAST, Brunel University London,
Uxbridge UB8 3PH, UK
Tel: +44 1895 266406
Email: zhongyun.fan@brunel.ac.uk

Mechanism for Si Poisoning of Al-Ti-B Grain Refiners in Al-Alloys

Abstract

Al-5Ti-1B is the most widely used grain refiner for Al-alloys. However, it is not effective for grain refining Al-alloys containing more than 3 wt.% Si. This adverse effect of Si is referred to as Si poisoning. In spite of extensive experimental and theoretical investigations in the past decades, the exact mechanism for Si poisoning is still not clear. In this work, the state-of-the-art electron microscopy was performed to investigate the mechanism for Si poisoning. Our experimental results suggest that Si segregates preferably to the TiB_2/Al-Si melt interface and the pre-existing Al_3Ti 2-dimensional compound (2DC) layer on TiB_2 surface dissolves into the Al-Si melt. Based on the experimental results, we have postulated a new mechanism for Si poisoning: interfacial segregation of Si leads to enrichment of Si at the TiB_2/Al-Si melt interface, and this in turn makes the pre-existing Al_3Ti 2DC on the TiB_2 surface unstable and dissolve gradually in the melt, resulting in a loss of TiB_2 nucleation potency and hence a decreased total number of potent TiB_2 particles available for heterogeneous nucleation and grain initiation and consequently an increased grain size. This mechanism for Si poisoning can explain consistently the experimentally observed phenomenon reported in the literature.

Keywords: Solidification; Heterogeneous nucleation; Grain refinement; Si poisoning.

1. Introduction

A grain refined microstructure is usually desirable for Al-alloy castings, since it not only facilitates the casting processes, but also improves mechanical performance of the alloys through reduced cast defects, such as macro-segregation, hot tearing and porosity. In the Al industry, a common foundry practice for grain refinement is addition of grain refiner prior to casting processes, with Al-5Ti-1B (all the alloy compositions are in wt.% unless stated otherwise) being the most widely used commercial grain refiner. Since the introduction of Al-Ti-B based grain refiners in early 1950s, [1] extensive experimental investigations and theoretical studies have been carried out to understand the underpinning mechanisms for grain refinement. [2-7] It is now generally accepted that promoting heterogeneous nucleation of numerous αAl grains on TiB_2 particles is responsible for grain refinement. Various hypotheses have been proposed to explain the mechanisms of heterogeneous nucleation in the Al-TiB_2 system. [3-7] It is only until very recently to realize that the formation of an atomic layer of Al_3Ti 2-dimensional compound (2DC) on the (0 0 0 1) TiB_2 surface is responsible for the high potency of the TiB_2 particles for nucleation of αAl grains. [8]

The presence of alloying elements has long been recognized as one of the important factors for grain refinement by providing growth restriction. However, this may not be true for all the elements. For instance, Al-5Ti-1B becomes ineffective for grain refinement when certain elements are present in the alloy melt, such as Zr, [9-14] Li, [15-16] Cr, [17-18] and high levels of Si. [19-34] The negative effect of solute elements on grain refinement is referred to as "poisoning" in the literature. One of the main explanations to the poisoning effect is that the

interaction between solute elements and TiB_2 particles leads to the decrease in nucleation potency of the TiB_2 particles. [35] Our recent research work on Zr poisoning disclosed that the presence of Zr in the melt results in the dissolution of the pre-existing Al_3Ti 2DC layer (formed during the grain refiner production process) and the formation of a Ti_2Zr 2DC atomic layer on TiB_2 surface, which is responsible for the reduced potency of TiB_2 for heterogeneous nucleation of αAl. [36]

The phenomenon of Si poisoning has been observed in Al-Si alloys containing more than 3% Si inoculated with Al-5Ti-1B grain refiner. [19-23, 30-32] Sigworth and Guzowaski [20] and Johnsson *et al* [21-22] showed that, with inoculation by Al-5Ti-1B, the grain size of Al-Si alloys first decreased slightly and then increased with increasing Si content with a minimum value at ~3% Si. A number of studies subsequently confirmed the poisoning effect of Si. [23-34] In addition, it was found that at a given processing temperature and a given Si concentration (> 3%), the grain size increases with increasing holding time of the melt prior casting. [32] Furthermore, Si poisoning has also been reported in Al-Si alloys without the addition of Al-5Ti-1B grain refiner. It was found that the grain size of un-inoculated Al-Si alloys began to increase after reaching to a minimum value at ~3% Si. [26, 29-31, 34]

Overcoming Si poisoning has been a significant research topic in the past decades. The major approaches include: (i) higher addition level of hyper-stoichiometric (the stoichiometric weight ratio of Ti:B = 2.2:1) Al-Ti-B master alloys; [32-33, 37] (ii) modification of grain refiner composition, such as Al-2.2Ti-1B, Al-3Ti-3B and Al-1Ti-3B; [37-41] and (iii) development of new grain refiners based on the other alloy systems, such as Al-Ti-C, [37, 42-43] Al-Ti-B-C, [44] Al-B [37,40,45-47] and Al-Nb-B. [48-50] For instance, addition level of as high as 0.6% (typically 0.1% for a standard practice in industry) of Al-5Ti-1B grain refiner was shown to result in a fully refined structure for Al-7Si alloys. [32, 33] In addition, some newly developed alternatives, such as Al–3Ti–3B and Al–1Ti–3B (sub-stoichiometric), have been reported to provide a better grain refinement performance than the conventional Al–5Ti–B refiner. [37-40] Furthermore, binary Al-B system without Ti involved, Al-3B for instance, was shown to offer a better refining performance than Al-5Ti-1B. [33, 45-47] More recently, Al-2Nb-2B based grain refiner were claimed to offer good performance in grain refinement of Al-Si alloys with poisoning resistance. [48-50] Effect of trace elements on refining effectiveness of Al-Ti-B based refiner has also been investigated. It was noted that some elements, such as Mg and Sr etc., were shown to counteract Si poisoning. [32, 41, 51]

A number of hypotheses were proposed to explain the mechanism for Si poisoning, although no consensus has been reached so far. One school of thoughts is the formation of Ti-Si or Ti-Si-Al compounds on the TiB_2 surface. It was postulated that formation of the silicides by interaction between TiB_2 and solute Si made the nucleant particles less potent, [20, 21, 35, 52-54] although there was little direct experimental evidence for this mechanism. For instance, formation of Ti-Si compounds at the TiB_2/αAl interface was reported only in metallic glass ($Al_{80}Ni_{10}Cu_8Si_2$ alloy containing up to 0.09%Ti), [52-54] but not in Al melt containing high Si content. Thermodynamic analysis for formation of various silicides was carried out. [35, 55] It was reported that, with increasing Si content, the Ti level required for $TiSi_2$ formation is reduced. [55] In addition, based on thermodynamics and lattice matching, [35] it was suggested that, among all the possible Ti-Si or Ti-Si-Al compounds, Ti_5Si_3 was the likely one to form on TiB_2 surface causing poisoning effect. Another school of thoughts involves the increased

growth velocity of αAl. Due to a reduced growth restriction caused by formation of titanium silicides, [56] the growth velocity of αAl would increase. Thermodynamic calculations also showed that, with high level of Si and excess Ti in Al-Si melt, the growth restriction parameter Q would be greatly affected by strong exothermic interaction between the solutes Si and Ti. [57] "Coincidently" at ~3% Si, a morphological transition from globular (cellular) to dendritic for αAl was observed. [29] It was thus suggested that highly branched dendrites, which grew more rapidly, had a smaller dendrite tip radius and were thus able to disperse solute sideways as opposed to globular tips which pushed solute ahead of the solid/liquid interface. Arguably Si poisoning was attributed to the increase in the growth velocity of the dendrite arms due to a decreased tip radius with increasing Si content, [22, 23, 58] although the similar morphological transition was observed in Al-Cu alloys. [30, 59] Other hypotheses involve the change of solid/liquid interfacial energy, [29, 32, 60] solidification range [24, 30, 31] despite limited understanding, [61] and reduced peritectic temperature for the formation of a ternary aluminide (Al-Ti-Si) layer. [37]

Si poisoning has been a well-known phenomenon observed in various Al-Si alloys for decades. Although a number of explanations have been proposed, the exact cause remains elusive. In this work, based on the confirmation of Si poisoning in Al-Si binary alloys solidified at a constant cooling rate, extensive electron microscopy was carried out on the collected TiB_2 particles from Al-Si melts, focusing on TiB_2/αAl interfaces to reveal any possible structural and chemical modification of the TiB_2 particles caused by interactions between solute Si or impurity elements and the introduced TiB_2 particles. Composition profiles of Si and relevant impurities were established at local areas across the TiB_2/αAl interface by high resolution STEM and high resolution Super-X EDS analysis. Based on the experimental findings of Si segregation at TiB_2/αAl (liquid) interface and the subsequent influence on the potency of TiB_2 particles for heterogeneous nucleation of αAl, we aim to identify the operating mechanism for Si poisoning of Al-Ti-B based grain refiners, providing elucidation of experimental observations. Understanding of mechanism for the poisoning effect provides the basis for developments of effective methods and alternative grain refiners to alleviate and overcome eventually the negative poisoning effect.

2. Experimental

2.1. Raw Materials

Commercial purity aluminum (CP-Al) and Al-50Si master alloy were used in this work. Al-Si alloys containing up to 10% Si were prepared using the CP-Al and Al-50Si master alloy in a resistance furnace at 750°C with isothermal holding for an hour after melting. TiB_2 particles were introduced by addition of 0.2% commercial Al-5Ti-1B grain refiner rods, supplied by LSM (Rotherham, UK). The chemical compositions and impurity levels of the materials used in this work are given in Table 1.

Table 1 Compositions (wt.%) of materials used in this work.

Alloy	Si	Ti	B	Fe	V	Zn	Ni	Cu	Cr	Al	Supplier

CP-Al	0.03	0.006	--	0.08	--	0.003	0.005	0.001	0.001	Bal.	Norton
Al-50Si	49.90	0.02	--	0.60	--	0.02	0.01	0.03	0.01	Bal.	Avon Metals
Al-5Ti-B	0.08	4.8	0.85	0.09	0.04	--	--	--	--	Bal.	LSM

142

143 2.2. Casting and grain size assessment

144 The grain size of the Al-Si alloys was assessed using the standard TP-1 test [62] which
145 provides a consistent cooling rate of ~3.5 K/s at the central region of the transverse section 38
146 mm from the bottom of the TP-1 cast ingot. After the addition of 0.2% Al-5Ti-1B grain refiner,
147 the Al-Si melt was holding for further 30 min. at 750 °C and stirred in every 10 minutes, and
148 then poured into the pre-heated TP-1 mold (350 °C) which was then cooled by water spray
149 with a flow rate of 3.8 l/min. For comparison, TP-1 tests were also conducted for CP-Al with
150 and without inoculation with the commercial Al-5Ti-1B grain refiner.

151 Examination of grain structure and quantification of grain size of the solidified TP-1 samples
152 were carried out at the transverse section 38 mm from the base, and the longitudinal section of
153 the lower part of the TP-1 ingots. The specimens for the quantitative metallography were
154 prepared following the standard procedures, subjected to a final polishing before anodizing
155 using Barker's reagent (5 ml HBF4 + 200 ml distilled water). A Zeiss optical microscope fitted
156 with the Axio Vision 4.3 image analysis system was used for the grain size measurement. For
157 each of the measurement by the mean linear intercept technique, the average of at least 500
158 grains from areas covering the whole transverse section of the TP-1 ingot was taken for the
159 quantification of the grain size under the given casting conditions.

160

161 2.3. SEM and high resolution TEM/STEM

162 In order to facilitate examinations of TiB_2 particles and their interfaces with αAl by electron
163 microscopy, a pressurized melt filtration technique was used to collect the TiB_2 particles in the
164 Al-Si melts inoculated with Al-5Ti-1B grain refiner. In this process, the prepared CP-Al or Al-
165 Si alloy melt containing TiB_2 particles was transferred into the crucible in the pressure chamber
166 of the melt filtration unit. Argon was introduced to force the melt to flow through a porous
167 ceramic filter attached to the bottom of the crucible. TiB_2 particles were thus collected
168 immediate above the filter. The solidified material above the filter, which contained the locally
169 concentrated TiB_2 particles, was subjected to sampling. A detailed description of melt filtration
170 for collection of particles can be found elsewhere. [63, 64]

171 The collected TiB_2 particles, their surface and interface with αAl in particular, were examined.
172 Scanning electron microscopy (SEM) was performed using a Carl Zeiss Crossbeam 340
173 microscope equipped with energy dispersive x-ray spectroscopy (EDS). Thin foil specimens for
174 transmission electron microscopy (TEM) and scanning transmission electron microscopy
175 (STEM) were prepared from 3 mm diameter discs sliced from the filtered residue material. The
176 discs were manually ground to a thickness less than 60 μm before further thinning by argon ion
177 beam milling using a Gatan precision ion polishing system (PIPS) under a voltage of 1.0-5.0

kV and an incident beam angle of 3-5°. High resolution TEM examination was conducted on a JEOL 2100F microscope operated with an accelerating voltage of 200 kV. Atomic resolution STEM with Z contrast high-angle annular dark filed (HAADF) imaging was carried out on an aberration (Cs)-corrected FEI Titan 80-200 instrument equipped with Super-X energy dispersive x-ray spectroscopy (Super-X EDS) system, operated with an accelerating voltage of 200 kV. High resolution elemental mapping by STEM/Super-X EDS was conducted to obtain compositional profiles across TiB_2/αAl interface.

3. Results

3.1. Si poisoning of Al-5Ti-1B grain refiner

Figure 1 shows the typical macrostructures of CP-Al, Al-2.0Si and Al-8.4Si alloys solidified under the TP-1 test conditions. As expected, the addition of 0.2% Al-5Ti-1B grain refiner resulted in a significant grain refinement of CP-Al, transforming the coarse columnar grain structure (Figures 1a and 1b) into a fine and fully equiaxed one (Figures 1c and 1d). Similarly, a considerably refined and fully equiaxed grain structure was obtained for Al-2.0Si alloy inoculated with the grain refiner, as shown in Figures 1e and 1f. However, Al-8.4Si alloy inoculated with the same amount of the grain refiner showed a coarse and equiaxed grain structure (Figures 1g and 1h). The optical micrographs in Figure 2 show the microstructures of Al-2.0Si and Al-8.4Si alloys inoculated with the Al-5Ti-1B grain refiner. The average grain size of the primary αAl phase for Al-2.0Si alloy is 195±22 μm, being comparable to 202±26 μm for the refined CP-Al. However, the grain size is 686±73 μm for the inoculated Al-8.4Si alloy, which is considerably larger than that for the inoculated Al-2.0Si alloy. In addition, there is also clear difference in grain morphology between Al-2.0Si and Al-8.4Si alloys. The primary αAl has a typical rosette morphology for the inoculated Al-2.0Si alloy (Figure 2c), but a well-developed dendritic morphology for the inoculated Al-8.4Si alloy (Figure 2d).

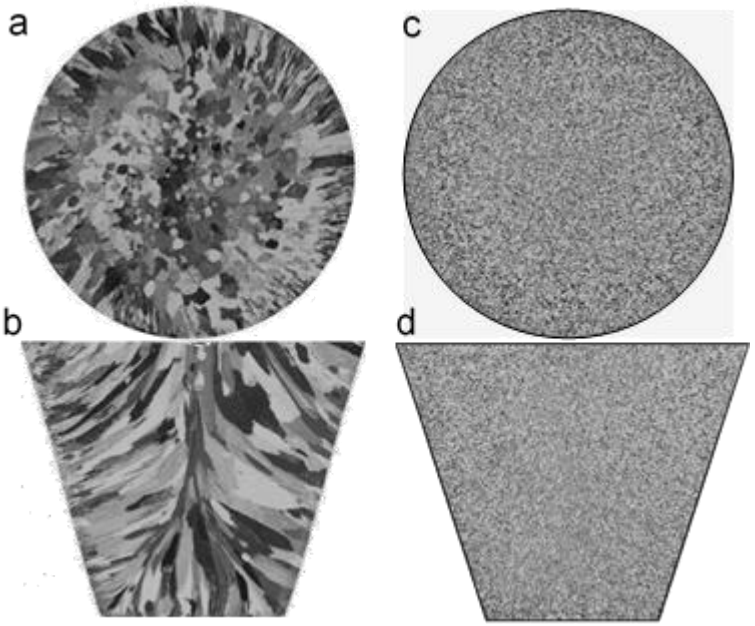

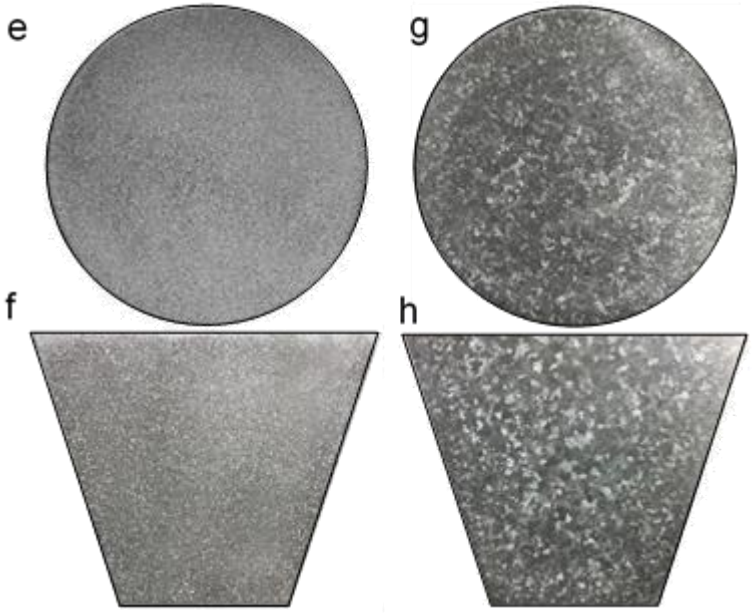

Fig. 1 Macrographs showing grain structures of TP-1 test samples on (a, c, e, g) transverse and (b, d, f, h) longitudinal sections of (a, b) CP-Al with no addition of grain refiner, (c, d) CP-Al, (e, f) Al-2.0Si and (g, h) Al-8.4Si alloys with addition of 0.2wt% commercial Al-5Ti-1B grain refiner.

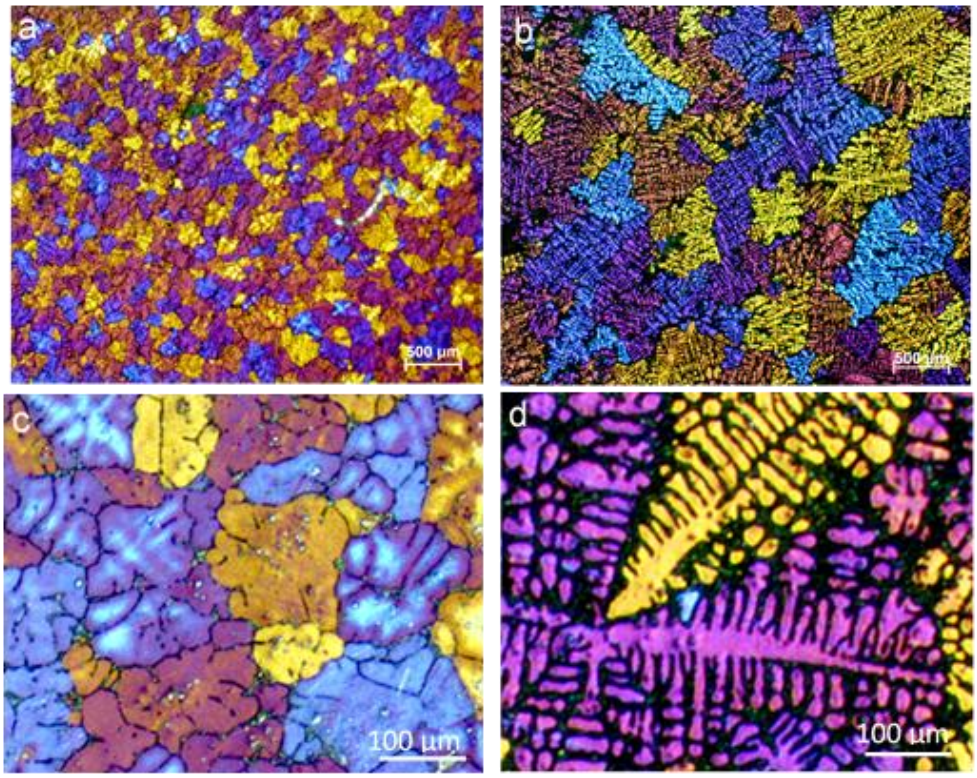

Fig. 2 Optical micrographs showing (a, b) general view of grain structures of TP-1 test samples of (a) Al-2.0Si and (b) Al-8.4Si alloy inoculated with 0.2 wt% Al-5Ti-1B, and (c, d) morphological transition from cellular to dendritic for the primary αAl with Si concentration increasing from (c) 2.0 wt% to (d) 8.4 wt%. The average grain size of αAl is measured to be 195±22 µm and 686±73 µm for Al-2.0Si and Al-8.4Si, respectively.

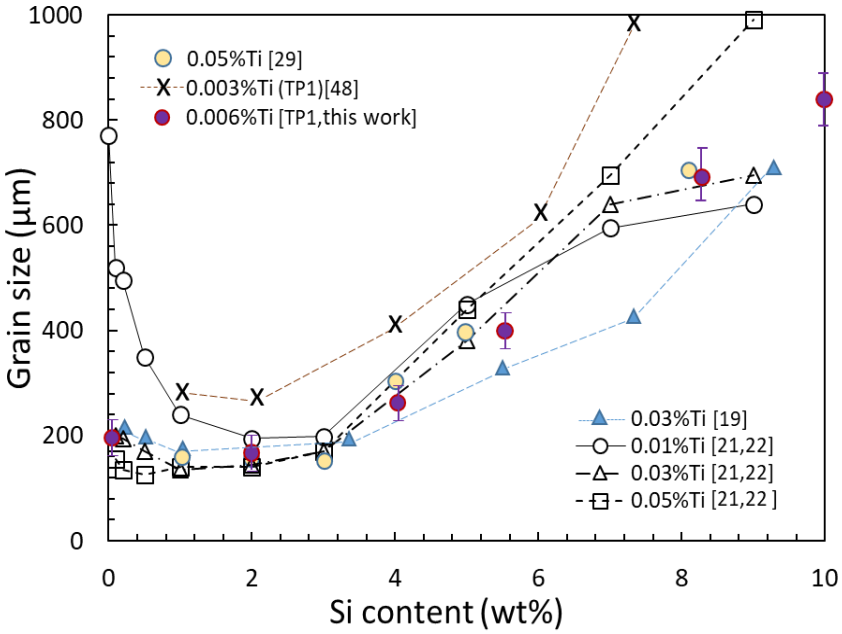

Fig. 3 Experimentally measured grain size of the primary αAl of hypoeutectic Al-Si alloys inoculated with Al-5Ti-1B grain refiner as a function of Si concentration, together with the representative data found in the literature.

The experimentally measured grain size is plotted in Figure 3 as a function of Si concentration, being compared with the representative experimental data found in the literature. In agreement with previous studies, the present work confirms the variation in grain size of Al-Si alloys with changing Si content, although the absolute values of grain size vary, probably due to the differences in the addition level of grain refiner, alloy composition, impurity level and solidification conditions in the different studies. All the experimental observations show in general that, when inoculated with Al-5Ti-1B grain refiners, grain size of hypoeutectic Al-Si alloys decreases slightly until ~3% Si and then increases with further increase of Si content.

3.2 TiB_2 particles added to Al-Si alloy melts

TiB_2 particles collected from the Al-Si alloy melt were subjected to extensive examinations by various microscopic techniques. The reference point for this study is the original state of the TiB_2 particles from the commercial grain refiner. Such TiB_2 particles are potent substrates for heterogeneous nucleation of αAl due to the presence of Al_3Ti 2DC layer on their (0 0 0 1) surface. [8, 36] There exists a well-defined orientation relationship (OR) between TiB_2 and αAl: [8, 36]

$$(0\ 0\ 0\ 1)\ [1\ 1\ -2\ 0]\ TiB_2\ //\ (1\ 1\ 1)\ [0\ -1\ 1]\ \alpha Al \qquad \text{(OR1)}$$

which serves as hard evidence for the nucleation of αAl on TiB_2 substrate.

Figure 4a shows the typical hexagonal morphology of the TiB_2 particles collected from the Al-8.4Si alloy melt inoculated with 0.2% Al-5Ti-1B. Compared with the original TiB_2 particles from the commercial grain refiner, [65] there was no visible change in morphology and size

after they were added to the melt and isothermally hold at 750°C. Figure 4b is a TEM bright field image showing the sharp TiB_2/Si interfaces at a higher magnification. Extensive high resolution TEM examination of multiple TiB_2 particles focusing on both TiB_2/αAl and TiB_2/Si interfaces revealed no evidence for the formation of any 3D bulk phase at the interfaces. Examples are given in Figures 4c and 4d, where sharp and smooth TiB_2/αAl (Figure 4c) and TiB_2/Si (Figure 4d) interfaces are evident at atomic scale.

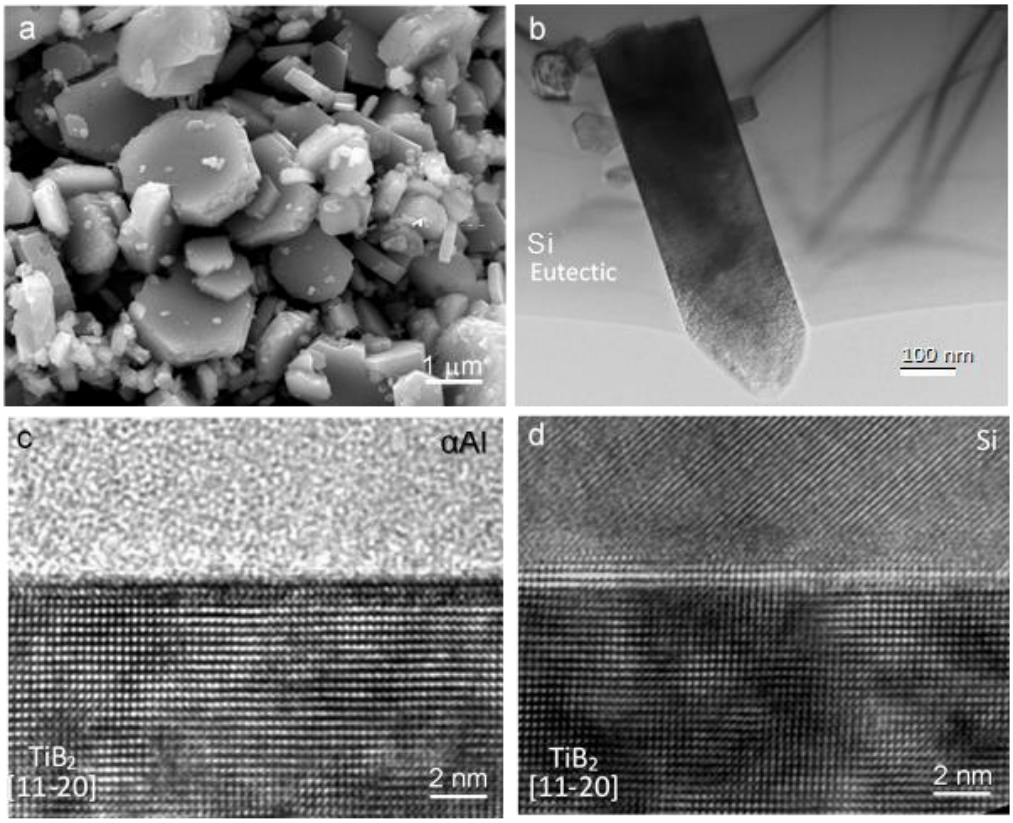

Fig. 4 (a) SEM and (b) TEM bright field image showing the morphology of TiB_2 particles collected from Al-8.4Si alloy melt inoculated with 0.2 wt% Al-5Ti-1B grain refiner, indicating the typical hexagonal shape of TiB_2 and its sharp surface; and (c, d) high resolution TEM images showing sharp and smooth (c) TiB_2/αAl and (d) TiB_2/Si (eutectic) interfaces at atomic scale.

TEM/STEM examinations showed that the majority of TiB_2 particles in Al-2.0Si and Al-8.4Si alloys were not in any defined OR with the adjacent αAl, indicating that the majority of the added TiB_2 particles did not participate in grain initiation of αAl during solidification. This is consistent with the conclusion derived from the free growth model that only less than 1% of the added TiB_2 particles are active for grain initiation. [65] TEM/STEM examination of multiple TiB_2 particles showed that the well-defined OR1 between TiB_2 and αAl was readily observed in the Al-2.0Si sample, as shown in Figures 5a and 5b. Occasionally, OR1 is not followed, e.g., {1 1 1} planes of αAl being a few degrees away from being parallel to {0 0 0 1} planes of TiB_2, although [1 1 -2 0]TiB_2 and [0 -1 1]αAl zone directions remain to be parallel to each other. As shown in Figures 5c and 5d, it is found by careful measurement through the fast Fourier

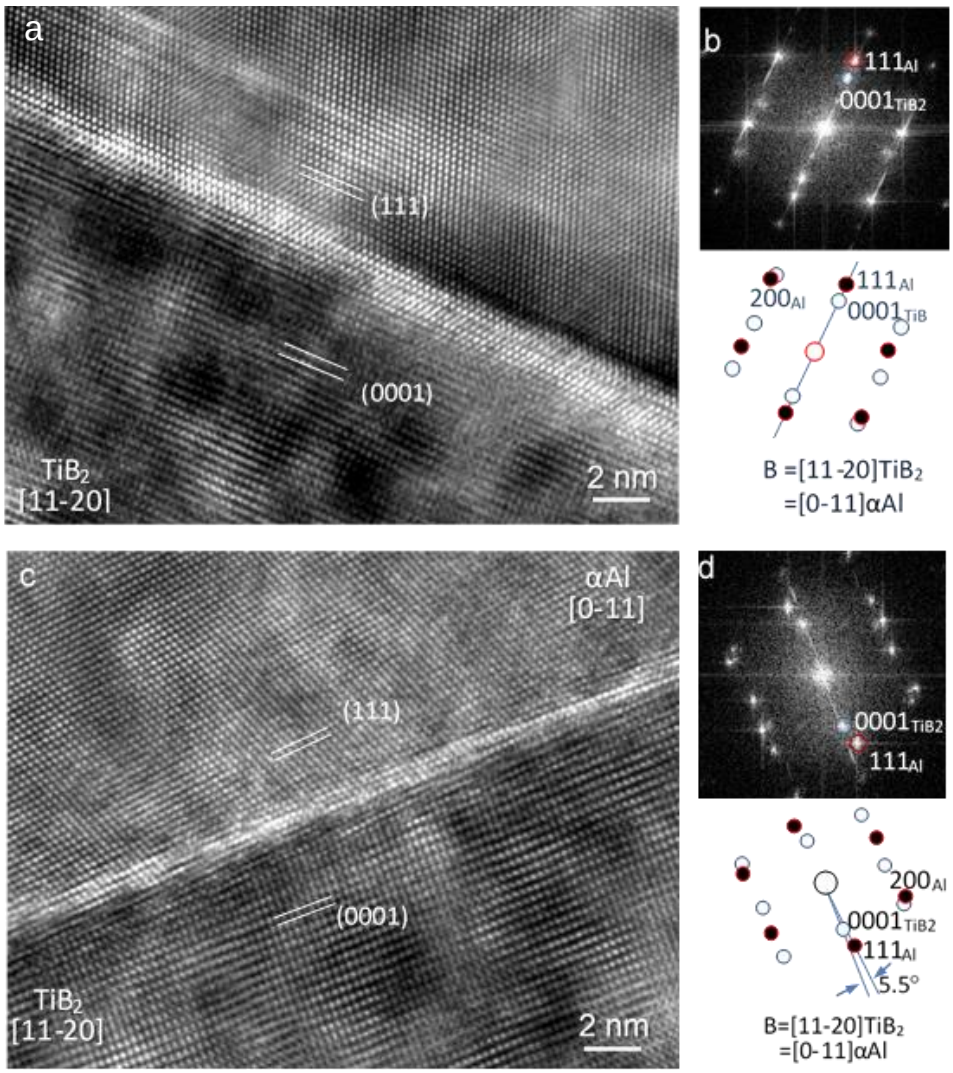

Fig. 5 (a, c) High resolution TEM images showing TiB_2/αAl interfaces in Al-2.0Si alloy sample where the TiB_2 particle and αAl are viewed along [1 1 -2 0]TiB_2 and [0 -1 1]αAl zone directions respectively; and (b, d) the corresponding fast Fourier transformation (FFT) patterns and their index showing that (1 1 1) αAl plane has a 5.5 degrees angle from (0 0 0 1)TiB_2 plane in (c, d).

transformation (FFT) patterns that (1 1 1)αAl plane is ~5.5° away from being parallel to (0 0 0 1) TiB_2 plane. This gives:

(0 0 0 1)TiB_2 ~5.5° (1 1 1) αAl, and [1 1 -2 0]TiB_2 // [0 -1 1]αAl. (OR2)

OR2 is actually equivalent to:

(0 0 0 1) [1 1 -2 0]TiB_2 // (5 5 4) [0 -1 1]αAl (OR2a)

In this case, the actual crystal plane of αAl which is parallel to (0 0 0 1)TiB_2 is (5 5 4), a relatively high index crystal plane of αAl.

However, TEM/STEM examinations of the TiB_2 particles collected from Al-8.4Si alloy melt inoculated with 0.2% Al-5Ti-1B grain refiner failed to find any well-defined OR between TiB_2 and αAl, although as many as 80 TiB_2 particles in total were examined in multiple thin foil

TEM specimens. TiB_2 and adjacent Al were occasionally found to be in some sort of orientations considerably deviated from OR1. For example, Figure 6 shows that, in one occasion, (1 1 1) αAl plane is far away from being paralleled to (0 0 0 1) TiB_2, and [1 1 0] αAl zone is not parallel to [1 1 -2 0] TiB_2 zone either. Instead, [1 -1 -2] αAl direction is parallel to [1 1 -2 0] TiB_2 direction, with a relatively high index (3 1 1) plane of αAl being about 11 degrees away from being parallel to (0 0 0 1) surface of TiB_2. Obviously this does not give a defined OR.

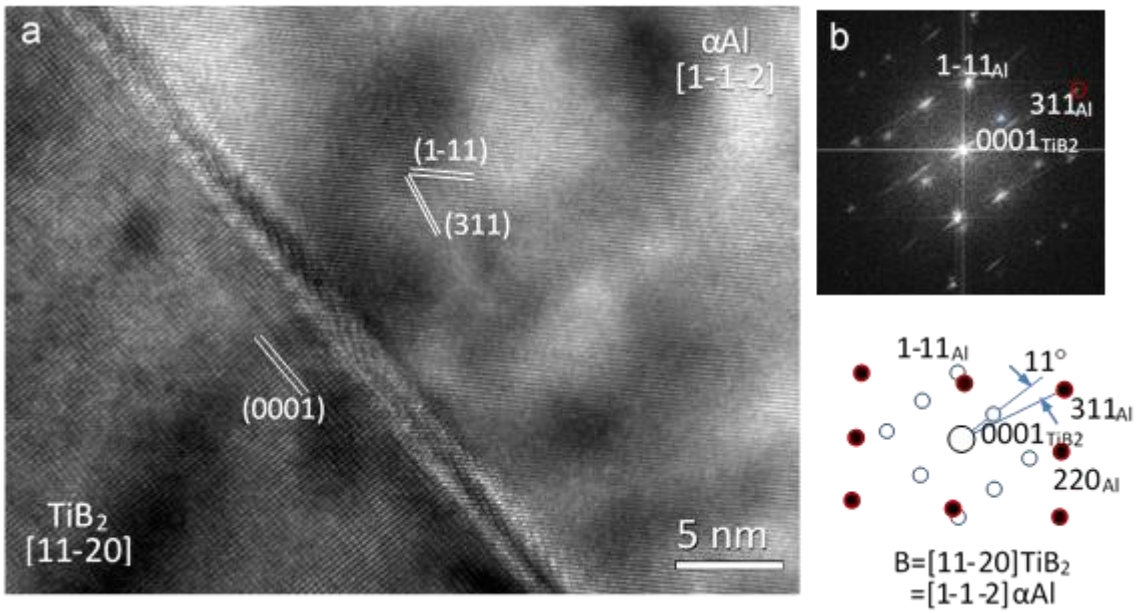

Fig. 6 (a) High resolution TEM image showing TiB_2/αAl interface of a TiB_2 particle in Al-8.4Si alloy sample where the TiB_2 particle and αAl grain are viewed along [1 1 -2 0]TiB_2 and [1 -1 -2]αAl zone directions, respectively, and (b) the corresponding fast Fourier transformation (FFT) pattern and its index.

Figures 7a and 7c are the high resolution STEM Z-contrast HAADF images showing the TiB_2/αAl interface of a TiB_2 particle in Al-8.4Si alloy, which suggest that there exists no bulk phase at the interface, verifying the above result from traditional high resolution TEM in Figure 4. Again, atomically sharp and smooth TiB_2/αAl interfaces were observed. In comparison with the TiB_2 in CP-Al sample where the Al_3Ti 2DC atomic layer is reserved (Figures 7b and 7d), [8] it is found that the pre-existing Al_3Ti 2DC layer is missing on the (0 0 0 1) TiB_2 surface for the TiB_2 particle collected from the Al-8.4Si sample (Figures 7a and 7c). High resolution STEM examination of multiple TiB_2 particles collected from the Al-8.4Si melt confirmed consistently the disappearance of Al_3Ti 2DC layer from TiB_2 surface.

However, a different situation was revealed for the TiB_2 particles collected from Al-2.0Si melt. Figure 8a is the high resolution STEM HAADF image across TiB_2/αAl interface with the TiB_2 particle being viewed along its [1 1 -2 0] zone direction. It is noted in Figure 8b, which is the enlargement of the rectangular region marked in Fig 8a, that the Al_3Ti 2DC remains on the left hand side of the (0 0 0 1) TiB_2 surface but is absent on the right hand side. As shown at higher magnification in Figure 8b, the brightness of the atomic columns of the Al_3Ti 2DC layer in the

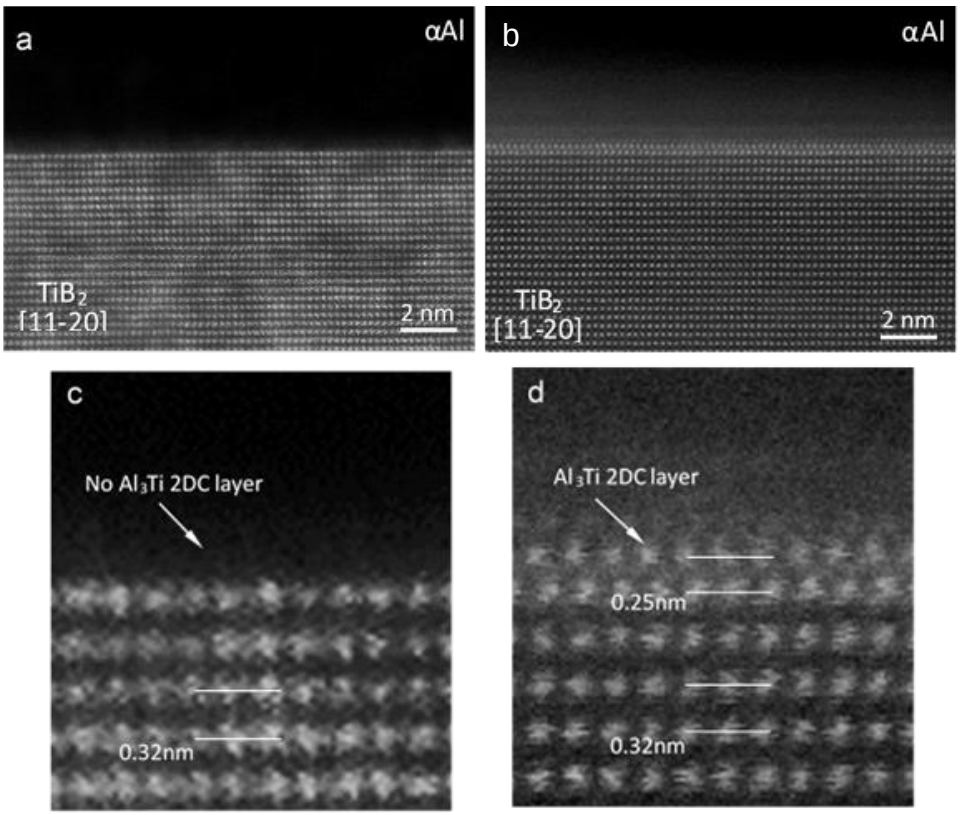

Fig. 7 High resolution STEM Z-contrast HAADF images of TiB_2/αAl interface showing (0 0 0 1) surface of TiB_2 viewed along [1 1 -2 0]TiB_2 zone direction in (a, c) Al-8.4Si alloy and (b, d) CP-Al. It is clear from (c, d) the HAADF images at higher magnifications that the Al_3Ti 2DC layer [8, 36] is missing on the (0 0 0 1)TiB_2 surface in (c) Al-8.4Si sample but present in (d) CP-Al sample.

STEM HAADF image is seen to start weakening at the position marked by the arrow and the atomic columns disappear completely towards the right hand side of the interface. This suggests that it is of significance that the Al_3Ti 2DC layer is not stable and tends to dissolve in the Al-Si melt. Figure 8 shows the on-going dissolution process of the 2DC layer, which occurs gradually after the TiB_2 particles were added to the Al-Si melt and holding at the processing temperature. In this work, Al_3Ti 2DC, which was formed on the surface of TiB_2 particles during production process of the commercial Al-5Ti-1B grain refiner, [8] was readily observed to remain on the surface of TiB_2 particles collected from the Al-2.0Si melt. This is in contrast to the situation in Al-8.4Si sample where the Al_3Ti 2DC layer was not at all observed, although multiple number of TiB_2 particles have been examined by high resolution STEM. That the possibility to observe the remaining Al_3Ti 2DC layer is considerably smaller in Al-8.4Si sample than that in Al-2.0Si indicates a faster dissolution rate for the 2DC layer in Al-Si melt with a higher Si content.

3.3 Si Segregation at TiB_2/αAl interface

Apparently Si concentration plays an important role in determining the dissolution kinetics of the Al_3Ti 2DC layer. It is therefore essential to study the chemical profiles across TiB_2/αAl

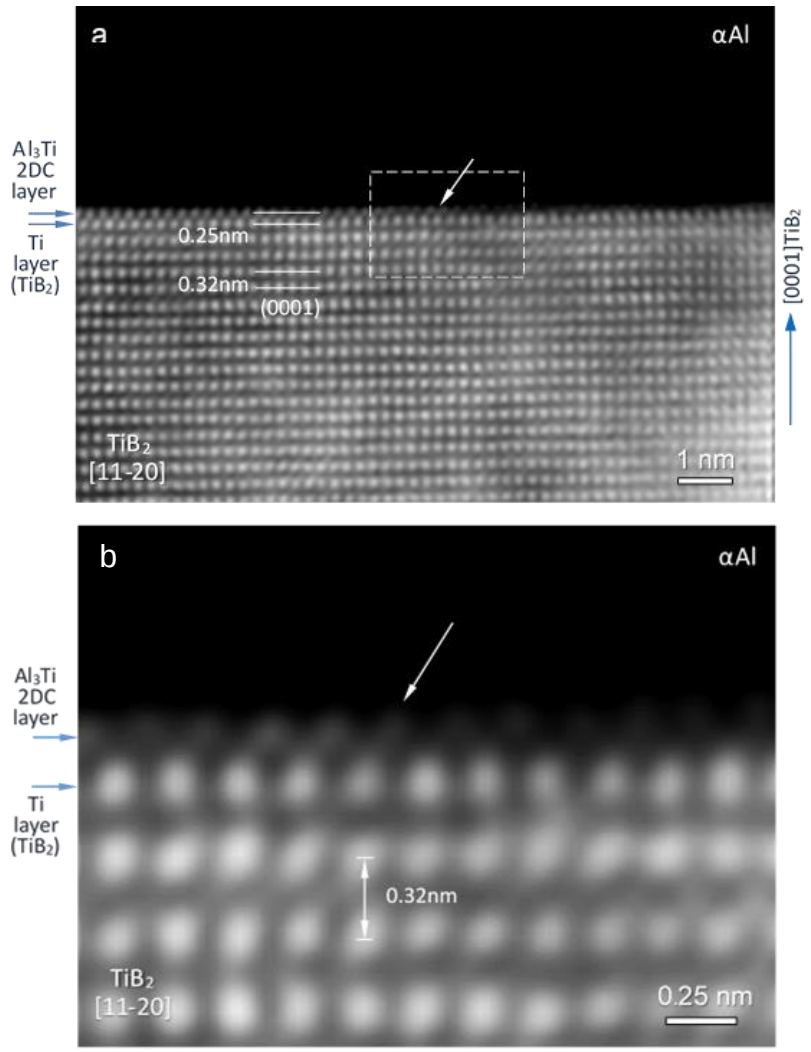

Fig. 8 High resolution STEM HAADF images across TiB_2/αAl interface viewed along [1 1 -2 0] TiB_2 zone direction showing (a) on-going dissolution (starting at the point marked by the arrow) of Al_3Ti 2DC layer on (0 0 0 1) surface of TiB_2 particle collected from Al-2.0Si alloy melt, and (b) enlargement of the marked rectangular region in (a).

interface. Figure 9 presents the EDS results obtained from Al-8.4Si sample. The STEM HAADF image in Figure 9a shows the TiB_2/αAl interface with no Al_3Ti 2DC layer covering the TiB_2 surface, and the corresponding Super-X EDS spectrum in Figure 9b taken from the local interface region marked in Figure 9a shows a major peak at energy 1.74 keV, i.e., the characteristic K_α peak of Si. More evidence of Si segregation at the TiB_2/αAl interface is provided by the elemental mapping of Si (Figure 9c), accompanied by those of Ti, Al and Fe, one of the main impurities in CP-Al (Table 1), as shown in Figures 9d-9f, respectively. It should be pointed out that Si segregation at TiB_2/αAl interface is hardly visible in terms of the brightness contrast in HAADF image due to the small difference of atomic number of Si (14) from that of Al (13). The EDS mapping did not suggest segregation of Fe at (0 0 0 1)TiB_2/αAl interface (Figure 9f). Further SuperX EDS analysis of other Al-Si alloys revealed that Si segregation at the TiB_2/αAl interface is common to all the Al-Si alloys. The elemental mapping in Figure 10, where the Al_3Ti 2DC layer was survived partially on the left-hand side of (0 0 0 1)

TiB_2 surface found in a TiB_2 particle collected from Al-2.0Si melt, indicates a similar Si segregation (Figure 10b) at the interface with and without the Al_3Ti 2DC.

Besides at {0 0 0 1}TiB_2/αAl interface, Si was found to segregate also to {1 0 -1 0}TiB_2/αAl interfaces, as shown by the EDS mapping in Figure 11. As a result, the TiB_2 particles added to Al-Si melt are actually coated by a Si-enriched layer of Al-Si melt where the Si concentration is higher than that in the bulk melt away from the TiB_2/αAl interface.

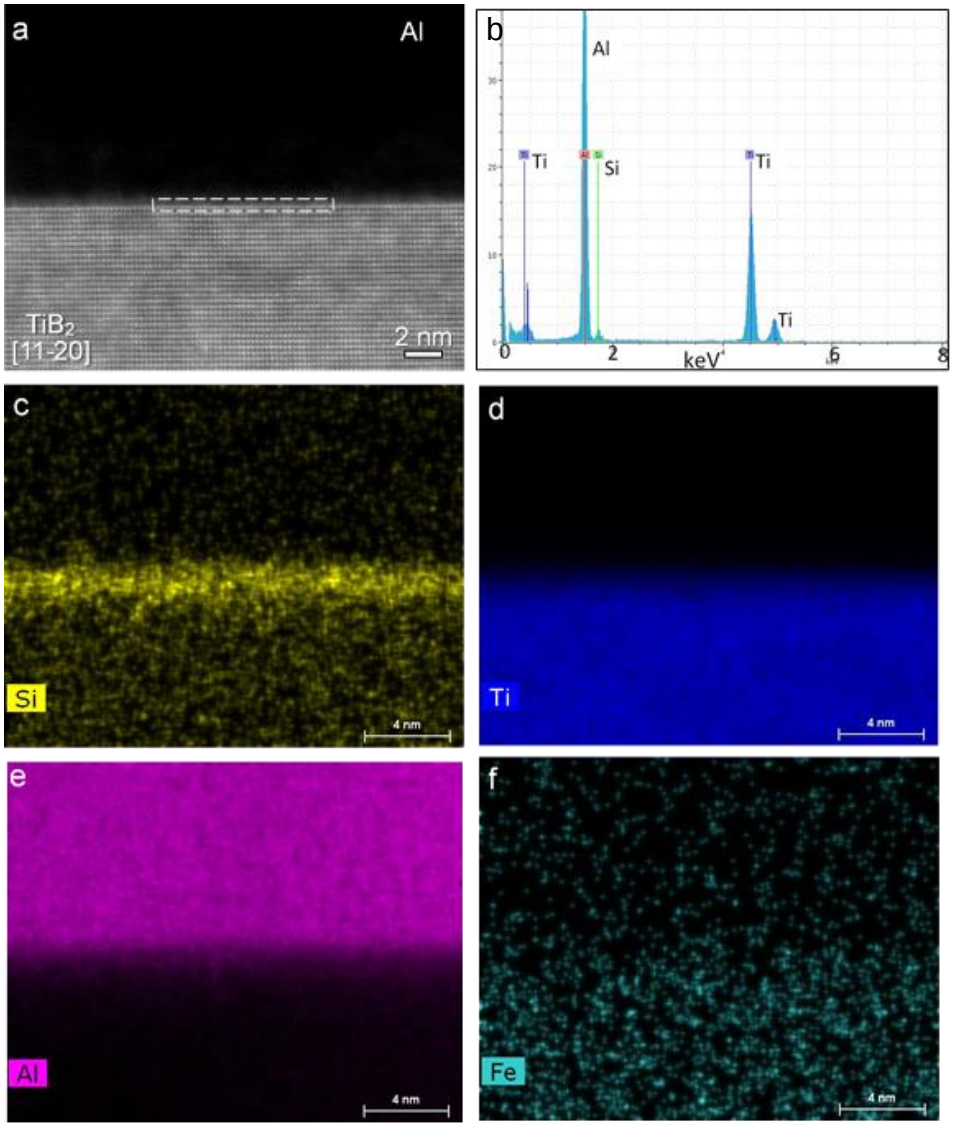

Fig. 9 (a) STEM Z-contrast HAADF image of TiB_2/Al interface in Al-8.4Si alloy sample inoculated with 0.2 wt% Al-5Ti-1B grain refiner; (b) Super-X EDS spectrum taken from the local region marked in (a) at the interface, and (c-f) Super-X EDS elemental mapping of (c) Si (yellow), (d) Ti (blue), (e) Al (purple) and (f) Fe (cyan) showing Si segregation at the interface.

4. Discussion

4.1 Facilitating TEM examination of nucleants by melt filtration

It is well accepted by the community that a well-defined OR observed by TEM is a direct evidence of nucleation of a solid on a nucleant. However, the difficulty comes from the

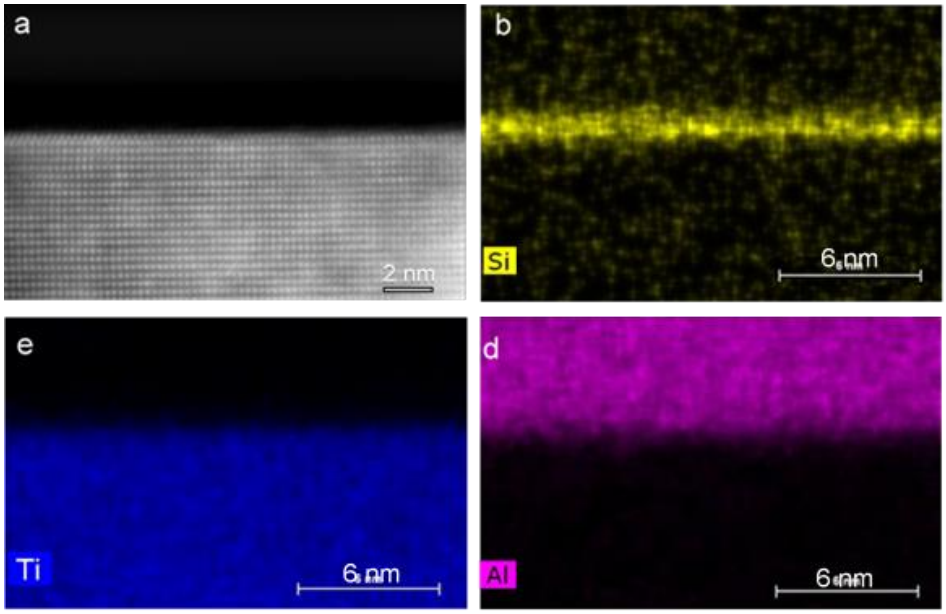

Fig. 10 (a) High resolution STEM HAADF image across TiB_2/αAl interface viewed along [1 1 -2 0] TiB_2 zone direction showing partially dissolved Al_3Ti 2DC layer on the (0 0 0 1) surface of the TiB_2 particle collected from Al-2.0Si melt, and (b-d) Super-X EDS elemental mapping of (b) Si (yellow), (c) Ti (blue) and (d) Al (purple) across the TiB_2/αAl interface showing that Si segregation is independent of the Al_3Ti 2DC.

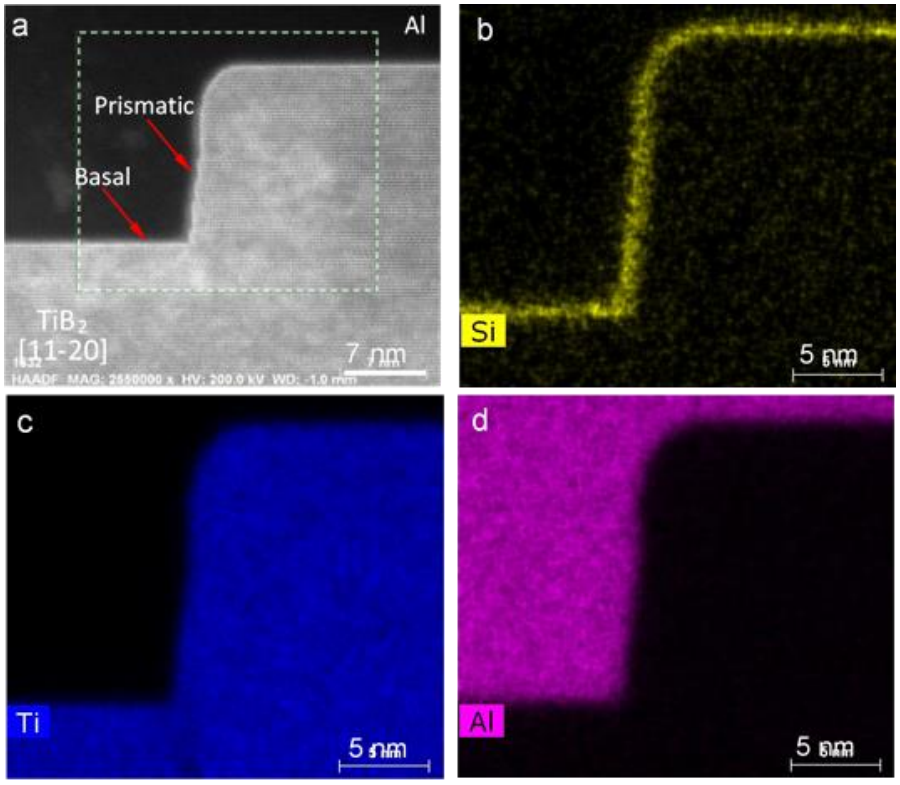

Fig. 11 (a) STEM HAADF image of TiB_2/Al interface in Al-8.4Si alloy inoculated with 0.2 wt% Al-5Ti-1B grain refiner, and (b-d) Super-X EDS mapping of (b) Si (yellow), (c) Ti (blue) and (d) Al (purple) across the TiB_2/αAl interface, showing Si segregation on both {0 0 0 1} basal and {1 0 -1 0} prismatic surfaces of TiB_2.

preparation of thin foil specimens for TEM examination. We take TiB_2 particles in Al-alloys as an example to demonstrate the challenge. If a TiB_2 particle (say 0.5 μm in size) has nucleated an Al grain (say 200 μm in size), it would sit inside the Al grain. The probability to find this TiB_2 particle on a 2D sectioning using the traditional metallography technique would be lower than one in a million, even lower probability to find this TiB_2 particle in the limited electron-transparent regions around the perforation of a ϕ3 mm disc for TEM examination. This explains why there has been no success in obtaining such an OR by TEM to evidence nucleation in the history of Al-Ti-B master alloys until the mid-1990s. Schumacher and Greer used devitrification of an Al-based metallic glass containing a high density of TiB_2 particles as an analogue to the nucleation of α-Al on TiB_2, and obtained successfully the first HRTEM images of TiB_2/Al interface in this analogue alloy. [66, 67] Successful examination of TiB_2/Al interface only became a routine when the melt filtration technique was used for TEM sample preparation in 2015. [8]

Pressurized melt filtration, as described previously, allows a significant increase of TiB_2 particle number density in a localized region of the melt, but it does not change either the particle potency or melt composition. According to the recent understanding of early stages of solidification, [68] the heterogeneous nucleation processes of the melt before and after filtering are exactly the same, although the increase in particle number density may leads to an increase grain initiation events, thus a finer grain size. Both increase in TiB_2 particle number density and decrease in grain size favor the promotion of the probability of successful TEM samples containing TiB_2/Al interface. So far, this technique has been successfully deployed to study the mechanisms of grain refinement, [8] Zr-poisoning [36] and Si-poisoning (this work), all related to TiB_2 particles in Al-alloys.

4.2 Si interfacial segregation and its effect on nucleation

Interfacial segregation of Si at the TiB_2/Al-Si melt interface is both theoretically plausible and practically feasible. Experimentally, Si segregation has been observed at TiB_2/melt interfaces in the literature under various conditions. [37, 52-54, 69] Khalifa *et al* observed Si segregation on surfaces of various inclusions in Al melt, including TiB_2 and Al_2O_3. [60] Even with a very low concentration as an impurity in NiAl/TiB_2 composite, a Si segregation layer about ~0.6 nm thick was detected at (0 0 0 1)TiB_2/matrix interface. [69] McKay *et al* [52-53] and Schumacher *et al* [54] also observed Si segregation on the surface of TiB_2 in amorphous Al-Si-Ni and Al-Cu-Ni-Si alloys. It is confirmed in this work that Si segregates to both the basal and prismatic surfaces of TiB_2 particles in Al-Si alloy melts (Figures 9, 10 and 11). Theoretically, interfacial segregation is driven by reduction of interfacial energy and can be described by the Gibbs adsorption isotherm. [70] Solute segregation at substrate/liquid interface has been demonstrated to change both interfacial energies and the wetting behavior, and therefore affects heterogeneous nucleation behavior. [71-73] Recently, Men and Fan [74] have applied the Gibbs adsorption isotherm to analyze solute segregation at substrate/liquid interfaces and showed that the interfacial solute segregation is governed by i) the difference in interfacial energies between the pure solute/substrate and pure solvent/substrate interfaces, ii) the heat of mixing of the solution, and iii) the difference in entropies of fusion between pure solute and solvent. Due to the lack of relevant input data in the literature, an accurate prediction of Si

segregation at the TiB_2/Al-Si melt interface is not possible. However, a qualitative analysis using the above model [74] does suggest that a significant amount of excess Si can segregate at the TiB_2/Al-Si melt interface. The higher the Si concentration in the melt, the more enrichment of Si at the interface is resulted.

Si segregation at the TiB_2/Al-Si melt interface leads to the formation of a 2-dimetional solution (2DS). Under the experimental conditions of this work, the high resolution TEM and STEM examination has confirmed that there is no formation of either 2D compound (2DC) or 3D bulk phase at the TiB_2/αAl interface (Figures 4 to 8), although Si segregation is clearly observed at the interface. According to the Gibbs adsorption isotherm, solute segregation driven by interfacial energy reduction occurs only in one or two atomic layers. It is therefore believed that Si enrichment at the interface is a 2-dimetional solution (2DS). In addition, it seems that the formation of Si-enriched 2DS occurs only in Al-Si melt containing sufficiently high Si concentration, since notable Si segregation at the TiB_2/melt interface was not observed in CP-Al which contains about 0.03% Si as one of the main impurities. [8, 36] This is different from the cases of interfacial segregation of Ti or Zr, where ordered Al_3Ti 2DC [8] and Ti_2Zr 2DC [36] were observed at the TiB_2/αAl interface at low concentrations of Ti or Zr in the melt, respectively. The formation of Si-enriched 2DS at the TiB_2/Al-Si melt interface is expected to play an important role in modifying the surface of TiB_2 particles, and therefore their potency for heterogeneous nucleation.

An important phenomenon revealed in this work is the dissolution of Al_3Ti 2DC layer which was formed on the TiB_2 surface during the fabrication of the commercial Al-5Ti-1B grain refiner. [8] The Al_3Ti 2DC layer is at least kinetically stable in CP-Al melt, with its dissolution rate in CP-Al being so slow that a visible effect on grain refinement was observed only after isothermal holding of the inoculated melt for a period of time up to 78 hours at 800°C. [8] However, it is clear from this work that the stability of Al_3Ti 2DC layer is considerably reduced when sufficiently high Si content is present in the Al melt. The Al_3Ti 2DC layer is readily observed to remain on some TiB_2 particles collected from Al-2.0Si melt (Figures 8 and 10) but hardly found on the surface of those TiB_2 particles collected from Al-8.4Si melt (Figures 7 and 9). This fact indicates that the Al_3Ti 2DC layer becomes thermodynamically and/or kinetically unstable and dissolves faster in a higher Si melt than in a lower Si melt. Furthermore, Figures 5 and 6 show that a well-defined OR1 and a slightly deviated OR2 between TiB_2 and αAl are found at low Si content (2.0%), but no defined OR is observed at high Si contents (8.4%) in this study, suggesting that a fewer number of TiB_2 particles had participated in grain initiation of αAl in the high Si melt, in comparison with that in the low Si melt. As the Al_3Ti 2DC layer is on the Ti-terminated (0 0 0 1)TiB_2 surface, the dissolution rate is actually dependent on the local Si content at the interface, which is expected to be much higher than that in the bulk melt due to the Si interfacial segregation. With a given level of Al-5Ti-1B addition and thus a fixed total number of the TiB_2 particles in the melt, more TiB_2 particles will lose their Al_3Ti 2DC layer when Si concentration is higher due to the correspondingly faster dissolution rate, and then the number fraction of those unaffected TiB_2 particles decreases. In comparison with Zr effect on stability of the Al_3Ti 2DC, dissolution of the Al_3Ti 2DC layer in Al-Si melt requires a much higher Si concentration and the dissolution rate is dependent on Si content, whilst 580 ppm (0.058%) Zr in Al melt is sufficient to make the Al_3Ti 2DC layer dissolve completely at a similar temperature. [36]

Dissolution of Al_3Ti 2DC layer results in a reduced potency of TiB_2 particles for heterogeneous nucleation of αAl. Nucleation and subsequent grain initiation events are dependent on the exact physical and chemical characteristics of the nucleant particles introduced to the alloy melt from grain refiner, and their subsequent interactions with the melt. After dissolution of the pre-existing Al_3Ti 2DC layer, heterogeneous nucleation of αAl takes place directly on the (0 0 0 1) surface of TiB_2, and the crystallographic matching is between {0 0 0 1}TiB_2 and {1 1 1}αAl according to OR1. The original small lattice misfit 0.09% at the interface between (1 1 1)αAl and Al_3Ti 2DC now becomes much larger (-4.22%) between (0 0 0 1)TiB_2 and (1 1 1)αAl [8, 36]. The lattice misfit is even larger (more negative) between TiB_2 and Al-Si 2DS because the lattice parameter of αAl will be reduced when Si is dissolved in it. For instance, the lattice misfit is increased to -4.30% as the lattice parameter 0.4049 nm for pure Al decreases to 0.4047 nm for Al-0.97Si solid solution. [75] Consequently, the original TiB_2 particles in the grain refiner lost their potency for heterogeneous nucleation of αAl in Al-Si melt with high enough Si contents.

4.3 Mechanism of Si poisoning

Based on the previous analysis, a new mechanism for Si poisoning can be postulated here:

- Preferential interfacial segregation of Si leads to enrichment of Si at the TiB_2/Al-Si melt interface. The higher the Si concentration in the melt, the more enrichment of Si at the interface is;
- The pre-existing Al_3Ti 2DC layer on the TiB_2 surface dissolves gradually in the melt, resulting in a loss of nucleation potency for the TiB_2 particles. The dissolution rate of the 2DC layer increases with the increase of Si content at the interface;
- The overall effect is a reduced total number of potent (at original state) TiB_2 particles available for heterogeneous nucleation and grain initiation of αAl, and hence an increased grain size.

This mechanism for Si poisoning is consistent with the previous experimental observations reported in the literature. Previous experiments and this work showed that, upon Si poisoning, the minimum grain size of Al-Si alloys appeared at ~3% Si. This is in agreement with the above mechanism. When Si content is less than 3%, the dissolution rate of Al_3Ti 2DC is slow and the majority of the added TiB_2 particles are not affected or only partially affected. Therefore, the number of TiB_2 particles reserving its original state is sufficient for grain refinement. In this case, growth restriction will prevail over Si poisoning, giving rise to a marginal decrease in grain size with increasing Si content until 3% Si. With further increase in Si content, Si interfacial segregation increases and thus the dissolution of Al_3Ti 2DC layer becomes faster, resulting in a rapid decrease in the number density of the potent TiB_2 particles, and therefore Si poisoning effect prevails over the growth restriction, leading to an increase in grain size.

The experimental observation of defined ORs between TiB_2 and Al (Figures 5 and 6) and dissolution of Al_3Ti 2DC (Figures 7-8) in this work suggest that the number density of potent nucleant particles decreases with increasing Si content beyond 3%. Khalifa *et al* [60] showed that, in Al-Si alloys containing 0.3-0.9% Si, most of TiB_2 particles observed were located

within Al grains rather than the grain boundaries or the inter-dendritic regions. In contrast, more TiB_2 particles in Al-6.4Si alloy were found to locate in inter-dendritic regions, confirming that the TiB_2 particles were inactive nucleant particles in the high-Si alloys. Recently, *in-situ* observation using synchrotron radiation technology showed directly that nucleation events decreased with increasing Si content in TiB_2-inoculated Al-Si alloys. [34] In Al-Si alloys inoculated with 0.33% Al-3Ti-1B, the nucleation frequency was found to be reduced by two order of magnitude from 137 s^{-1} to 1.1 s^{-1} when Si content increased from 1.0% to 9.0%. [34]

This mechanism also explains the dependence of Si poisoning on holding time and the addition level of Al-Ti-B grain refiner. [28, 32] Abdel-Reihim *et al* found that, with 0.1% Al-5Ti-1B addition, the grain size of Al-3.5Si alloy increased from about 240 μm to 320 μm when holding time increases from 10 min. to 60 min.. [28] Kori *et al* [32] showed that, the higher the Si content (>7%) and the longer the holding time, the larger the grain size was. For instance, the grain size of Al-10Si alloy inoculated with 0.2% Al-5Ti-1B was about 260 μm and 650 μm for holding times of 5 min. and 120 min., respectively. [32] In addition, they found that, with a high level of grain refiner addition, for instance 0.6% (6 times of the standard 0.1%), [32] grain refinement was achieved for high Si Al-Si alloys. The reason for stronger Si poisoning at a longer holding time is because longer holding time leads to more impotent TiB_2 particles and hence larger grain size. However, this decrease in number density of potent particles can be compensated by increased level of grain refiner addition.

Si poisoning was also reported to occur in un-inoculated Al-Si alloys with the minimum grain size occurring at a similar Si content (~3%) to that in the inoculated alloys. [26, 29-31, 34] Si poisoning in un-inoculated Al-Si alloys is believed to be related to Si interfacial segregation, despite different types of inoculants. As Prasad *et al* showed, [34] un-inoculated Al-Si alloys also exhibited a significant number of nucleation events, suggesting that nucleation was triggered by random oxide or impurity particles, in spite of their lower and different potencies than that of TiB_2. Si could segregate to the interfaces between these oxide particles and Al-Si melt, leading to reduction in their potency for nucleation and therefore poisoning.

Our previous work [8, 36] has shown that Ti and Zr atoms in Al melts segregate preferentially to TiB_2/αAl interface, resulting in the formation of Al_3Ti 2DC or Ti_2Zr 2DC layer, respectively. However, the effect of the two types of 2DC layer on heterogeneous nucleation is just opposite, with Al_3Ti 2DC enhancing nucleation while Ti_2Zr 2DC impeding nucleation. In this work, Si segregation at TiB_2/Al-Si melt interface results in dissolution of Al_3Ti 2DC, with the dissolution rate being dependent on Si concentration at the interface. It is demonstrated that interfacial segregation of solute elements can significantly alter the behavior of the substrate during heterogeneous nucleation process. From nucleation point of view, segregation of solute elements leads to either enhancement or impediment of heterogeneous nucleation. This makes it possible to manipulate the nucleation process by modification of substrates through deliberate segregation of certain elements.

5. Conclusions

1) Al-5Ti-1B grain refiner is not effective for grain refining Al-Si alloys with Si concentration higher than 3%. Under the TP-1 solidification conditions of this work, the

grain size of αAl is increased from 195±22 μm to 867±78 μm as Si content is increased from 2% to 10% in the hypoeutectic Al-Si alloys inoculated with 0.2% of Al-5Ti-1B grain refiner. The increase in grain size with Si content was accompanied by a morphological transition from cellular to dendritic for the primary αAl phase.

2) A well-defined orientation relationship (OR) between TiB_2 and αAl, (0 0 0 1) [1 1 -2 0] TiB_2 // (1 1 1) [0 -1 1] αAl, is observed for the TiB_2 particles collected from Al-2.0Si melt, but no defined OR is found for the TiB_2 particles in Al-8.4Si alloy melt.

3) Si segregates preferentially to the solid/liquid interface between TiB_2 and Al-Si melt on both the {0 0 0 1} basal and {1 0 -1 0} prismatic surfaces of TiB_2 particles.

4) The Al_3Ti 2DC layer formed on the TiB_2 surface during the grain refiner production process becomes unstable in Al-Si melt and therefore dissolves into the melt with time. The 2DC layer is readily found to remain on the surface of some of the TiB_2 particles in low Si (2.0%) samples but not observed on the particles in high Si (8.4%) samples, showing an increased dissolution rate at high Si contents.

5) There is no evidence of formation of 2D or 3D bulk phase at the TiB_2/αAl interface under the experimental conditions of this work. Segregated Si atoms stay in a thin layer of Al-Si melt at the interface as 2 dimensional solution (2DS).

6) A new mechanism for Si poisoning is proposed: Preferential interfacial segregation of Si leads to enrichment of Si at the TiB_2/Al-Si melt interface, and this in turn makes the pre-existing Al_3Ti 2DC on the TiB_2 surface unstable and thus dissolve gradually in the melt resulting in a loss of its nucleation potency. The overall effect is a reduced total number of potent TiB_2 particles available for heterogeneous nucleation and grain initiation of αAl, and hence an increased grain size.

7) This new mechanism is consistent with the experimental findings in the literature, such as grain size minimum at 3% Si, dependence of grain size on holding time and levels of grain refiner addition, Si poisoning of un-inoculated Al-Si melts, and so on.

Acknowledgements

The EPSRC is gratefully acknowledged for providing financial support under grant number EP/N007638 /1.

References

1. A. Cibula, *J. Inst. Metals*, 1951-52, vol. 80, pp 1-16.
2. D.G. McCartney, *Inter. Mater. Rev.,* 1989, vol. 34, pp. 247-260.
3. M. Easton and D. StJohn, *Metall. Mater. Trans. A*, 1999, vol. 30A, pp. 1613-1623.
4. B.S. Murty, S.A. Kori and M. Chakraborty, 2002, *Inter. Mater. Rev.*, vol. 47, pp. 3-47.
5. T.E. Quested, *Mater. Sci. Tech.*, 2004, vol. 20, pp. 1357-1369.
6. L. Greer, *J. Chem. Phys*., 2016, vol. 145, pp. 211704.1-211704.14.
7. M.A. Easton, M. Qian, A. Prasad, and D.H. StJohn, *Curr. Opin. Solid State Mater. Sci.*, 2016, vol. 20, pp. 13-24.

8. Z. Fan, Y. Wang, Y. Zhang, T. Qin, X.R. Zhou, G.E. Thompson, T. Pennycook and T. Hashimoto, *Acta Mater*., 2015, vol. 84, pp. 292-304.
9. G.P. Jones and J. Pearson, *Metall. Trans. B*, 1976, vol. 7B, pp. 223-234.
10. A.A. Abdel-Hamid, *Z. Metallkd*., 1989, vol. 80, pp. 643-647.
11. M. Johnsson, *Z. Metallkd*. 1994, vol. 85, pp. 786-789.
12. J.A. Spittle and S. Sadli, *Cast Metals*, 1995, vol. 8, pp. 247-253.
13. A. Arjuna Rao, B.S. Murty and M. Chakraborty, *Mater. Sci. Technol*., 1997, vol. 13, pp. 769-777.
14. M.A. Kearns, P. Cooper, *Mater. Sci. Technol*., 1997, vol. 13, pp. 650-654.
15. M.E.J. Birch, in: C. Baker, P.J. Gregson, S.J. Harris and C.J. Peers (eds.), *Aluminium-lithium Alloys III*, The Institute of Metals, London, 1986, pp. 152-158.
16. C.R. Chakravorty and M. Chakraborty, *Cast Metals*, 1991, vol. 4, pp. 98-100.
17. A. Arjuna Rao, B.S. Murty and M. Chakraborty, *Metall. Mater. Trans. A*, vol. 27A, pp. 791-800.
18. A. Arjuna Rao, B.S. Murty and M. Chakraborty, *Int. J. Cast Met. Res*., 1996, vol. 9, pp. 125-132.
19. J. A. Spittle, *Inter. J Cast Metals Res*., 2006, vol. 19, pp. 210-222.
20. G.K. Sigworth and M.M. Guzowaski, *AFS Trans*., 1985, vol. 93, pp. 907-912.
21. M. Johnsson, *Z. Metallk*., 1994, vol. 85, pp. 781-785.
22. M. Johnsson and L. Backerud, *Z. Metallk*., 1996, vol. 87, pp. 216-220.
23. P. Hoefs, W. Reif and W. Schneider, *Giesserei*, 1994, vol. 81, pp. 398-406.
24. M. Abdel-Reihim, N. Hess, W. Reif and M.E.J. Birch, *J. Mater. Sci*., vol. 22, pp. 213-218.
25. J.A. Spittle, J.M. Keeble and M. Al Meshhedani, in: R. Huglen (ed.), *Light Metals 1997*, TMS, Warrendale PA, 1997, pp. 795-800.
26. J.E.C. Hutt, D.H. StJohn, L. Hogan and A.K. Dahle, *Mater. Sci. Technol*., 1999, vol. 15, pp. 495-500.
27. L. Backerud and M. Johnsson, in: W. Hale (ed.), *Light Metals 1996*, TMS, Anaheim CA, 1996, pp. 679-685.
28. M. Abdel-Reihim, N. Hess, W. Reif and M.E.J. Birch, *J. Mater. Sci*., 1987, vol. 22, pp. 213-218.
29. Y.C. Lee, A.K. Dahle, D.H. StJohn and J.E.C. Hutt, *Mater. Sci. Eng. A*, 1999, vol. 259, pp. 43-52.
30. Y. Birol, *Inter. J. Cast Metals Res*., 2013, vol. 26, pp. 22-27.
31. Y. Birol, *Mater. Sci. Technol*. 2012, vol. 28, pp. 385-389.
32. S.A. Kori, B.S. Murty and M. Chakraborty, *Mater. Sci. Tech*., 1999, vol. 15, pp. 986-992.
33. S.A. Kori, V. Auradi, B.S. Murty and M. Chakraborty, *Mater. Forum*, 2005, vol. 29, pp. 387-393.
34. A. Prasad, S.D. McDonald, H. Yasuda, K. Nogita and D.H. StJohn, *J. Cryst. Growth*, 2015, vol. 430, pp. 122-137.
35. D. Qiu, J.A. Taylor, M-X. Zhang and P.M. Kelly, *Acta Mater*. 2007, vol. 55, pp. 1447-1456.
36. Y. Wang, C.M. Fang, L. Zhou, T. Hashimoto, X. Zhou, Q.M. Ramasse and Z. Fan, *Acta Mater*., 2019, vol. 164, pp. 428-439.
37. P.S. Mohanty and J.E. Gruzleski, *Acta Mater.,* 1996, vol. 44, pp. 3749-3760.
38. G.S.V. Kumar, B.S. Murty and M. Chakraborty, *J. Alloys Compd*., 2009, vol. 472, pp. 112-

120.
39. T. Wang, H. Fu, Z. Chen, J. Xu, J. Zhu, F. Cao and T. Li, *J. Alloys Compd*., 2012, vol. 511, pp. 45-49.
40. Y. Birol, *Mater. Sci. Technol*., 2012, vol. 28, pp. 481-486.
41. S.A. Kori, B.S. Murty and B.S. Chakraborty., *Mater. Sci. Eng. A*, 2000, vol. 283, pp. 94-104.
42. L. Yu, X. Liu, Z. Wang and X. Bian, *J. Mater. Sci*., 2005, vol. 40, pp. 3865-3867.
43. H. Zhao, H. Bai, J. Wang and S. Guan, *Mater. Charact*., 2009, vol. 60, pp. 377-383.
44. P. Li, S. Liu, L. Zhang and X. Liu, *Mater. Design*, 2013, vol. 47, pp. 522-528.
45. Y. Birol, *J. Alloys Compd*. 2012, vol. 513, pp. 150-153.
46. Y. Birol, *Mater. Sci. Tech*., 2012, vol. 28, pp. 363-367.
47. Z. Chen, H. Kang, G. Fan, J. Li, Y. Lu, J. Jie, Y. Zhang, T. Li, X. Jian and T. Wang, *Acta Mater*., 2016, vol. 120, pp. 168-178.
48. M. Nowak, L. Bolzoni and N. Hari Babu, *Mater. Design*, 2015, vol. 66, pp. 366-375.
49. L. Bolzoni, M. Nowak and N. Hari Babu, *Mater. Design*, 2015, vol. 66, pp. 376-383.
50. L. Bolzoni and N. Hari Babu, *Metall. Mater. Trans. A*, 2019, vol. 50A, pp. 746-756.
51. M.E.J. Birch, P. Fisher, in: T. Sheppard (ed.), *Aluminium Technology 86*, The Institute of Metals, London, 1986, pp. 117-124.
52. B.J. McKay, *Heterogeneous nucleation in Al-Si alloys*, PhD Thesis, University of Oxford, Oxford, UK, 2001.
53. B.J. McKay, P. Cizek, P. Schumacher and K.A.Q. O'Reilly, *Mater. Sci. Eng. A*, 2001, vol. 304-306, pp. 240-244.
54. P. Schumacher and B. J. McKay, *J. Non-Cryst. Solids*, 2003, vol. 317, pp. 123-128.
55. T.E. Quested, A.T. Dinsdale and A.L. Greer, *Mater. Sci. Tech*., 2006, vol. 22, pp. 1126-1134.
56. P.S. Cooper, A. Hardman, D. Boot and E. Burhop, in: P. Crepeau (ed.), *Light Metals 2003*, TMS, Warrendale PA, 2003, pp. 923-928.
57. T.E. Quested, A.T. Dinsdale and A.L. Greer, *Acta Mater*., 2005, vol. 53, pp. 1323-1334.
58. M. Johnsson, *Thermochim. Acta*, 1995, vol. 256, pp. 107-121.
59. J.E.C. Hutt, A.K. Dahle, Y.C. Lee and D.H. StJohn, in: C.E. Eckert (ed.), *Light Metals 1999*, TMS, Warrendale PA, 1999, pp. 685-692.
60. W. Khalifa, F. H. Samuel and J. E. Gruzleski, *Metall. Mater. Trans. A*, 2004, vol. 35A, pp. 3233-3250.
61. M.A. Easton, A. Prasad and D.H. StJohn, *Mater. Sci. Forum*, 2014, vol. 794-796, pp. 161-166.
62. Standard Test Procedure for Aluminum Alloy Grain Refiners (TP-1), The Aluminum Association, Washington, DC, 1990.
63. Z. Fan, Y. Wang, M. Xia and S. Arumuganathar, *Acta Mater*., 2009, vol. 57, pp. 4891-4901.
64. Y. Wang, Z. Fan, X. Zhou and G.E. Thompson, *Phil. Mag. Lett*., 2011, vol. 91, pp. 516-529.
65. A.L. Greer, A.M. Bunn, A. Tronche, P.V. Evans and D.J. Bristow, *Acta Mater*., 2000, vol. 48, pp. 2823-2835.
66. P. Schumacher and A.L. Greer, *Mater. Sci. Eng. A*, 1994, vol. A178, pp. 309-313.
67. P. Schumacher and A.L. Greer, *Mater. Sci. Eng. A*, 1994, vol. A181/A182, pp. 1335-1339.

68. H. Men and Z. Fan, *Metall. Mater. Trans. A*, 2018, vol. 49, pp. 2766-2777.
69. L. Wang and R.J. Arsenault, *Metall. Trans. A*, 1991, vol. 22A, pp. 3013-3018.
70. E. Hondros, M. Seah, S. Hofmann and P. Lejcek, in: R. Cahn, P. Haasen (eds.), *Physical Metallurgy*, North-Holland, Amsterdam, 1996, pp. 1201-1289.
71. J.W. Christian, *The theory of transformations in metals and alloys*, 3rd ed., Pergamon, Oxford, 2002.
72. B. Cantor, *Philos. Trans. R. Soc. London. A*, 2003, vol. 361, pp. 409-417.
73. Z. Fan, *Metall. Mater. Trans. A*, 2013, vol. 44A, pp. 1409-1418.
74. H. Men and Z. Fan, *Metall. Mater. Trans. A*, 2014, vol. 45A, pp. 5508-5516.
75. W.B. Pearson, *A Handbook of lattice spacings and structures of metals and alloys*, Pergamon Press, London 1958, p. 382.